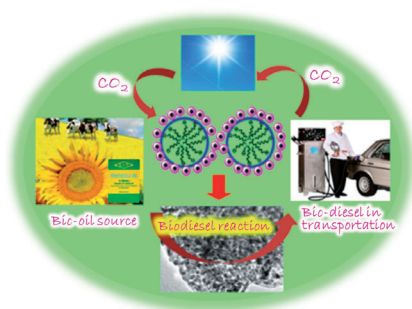


FULL PAPERS

Fasten your nanoparticles! Monodisperse nanoparticles are used as building blocks for a mesoscopic ZrO_2 nanoarchitecture by using the template as a fastening agent. Successive integration of the sulfate functionality into the porous framework makes the material a heterogeneous and recyclable catalyst for biodiesel production with a maximum biodiesel yield of 100%.



S. K. Das, S. A. El-Safty*

■ ■ - ■ ■

Development of Mesoscopically Assembled Sulfated Zirconia Nanoparticles as Promising Heterogeneous and Recyclable Biodiesel Catalysts



DOI: 10.1002/cctc.201300192

Development of Mesoscopically Assembled Sulfated Zirconia Nanoparticles as Promising Heterogeneous and Recyclable Biodiesel Catalysts

Swapan K. Das^[a] and Sherif A. El-Safty*^[a, b]

The nanoassembly of nearly monodisperse nanoparticles (NPs) as uniform building blocks to engineer zirconia (ZrO₂) nanostructures with mesoscopic ordering by using a template as a fastening agent was explored. The mesophase of the materials was investigated through powder X-ray diffraction and TEM analysis (TEM) and N₂ sorption studies. The TEM results revealed that the mesopores were created by the arrangement of ZrO₂ NPs with sizes of 7.0–9.0 nm and with broad interparticle pores. Moreover, the N₂ sorption study confirmed the results. The surface chemical analysis was performed to estimate

the distribution of Zr, O, and S in the sulfated ZrO₂ matrices. The materials in this study displayed excellent catalytic activity in the biodiesel reaction for effective conversion of long-chain fatty acids to their methyl esters, and the maximum biodiesel yield was approximately 100%. The excellent heterogeneous catalytic activity could be attributed to the open framework, large surface area, presence of ample acidic sites located at the surface of the matrix, and high structural stability of the materials. The catalysts revealed a negligible loss of activity in the catalytic cycles.

Introduction

Design and synthesis of porous crystalline metal oxides have been receiving great interest from the scientific community because of their versatile applications, such as solar cells, sensors, filters, and catalysts.^[1–7] Metal oxides fabricated through conventional sol–gel procedures are usually amorphous in nature, and their crystallization require high-temperature treatment, which often results in the collapse of mesostructures. Thus, their applications are limited.^[8] This limitation has motivated researchers in studying the formation of uniform crystalline-building nanounits that can be utilized as precursor artificial atoms for the fabrication of crystalline mesoporous structures in mild reaction conditions.^[9] Different routes, such as sol–gel, hydrothermal, and solvothermal crystallization, for the synthesis of metal oxide nanocrystals of various sizes and shapes and several nanoparticle (NP) assemblies with porous structures, such as TiO₂,^[10] CeO₂,^[4,11] CeO₂–Al(OH)₃,^[11] and SnO₂,^[12] have been reported. Chen et al. reported the hydrothermal fabrication of nanocrystalline zirconia (ZrO₂) by using a mixed-surfactant route with mixed tetragonal and monoclinic phases that exhibit both macropores and small mesopores.^[13] We recently prepared self-assembled mesoporous ZrO₂ NPs through evapo-

ration-induced self-assembly method through a nonaqueous route in the presence of Pluronic F127.^[14] However, the synthesis of crystalline porous self-assembled ZrO₂ NPs with controllable pore structures by using a template as a fastening agent is still a big challenge.

The utilization of porous solid materials in biodiesel production is very interesting because it correlates with environmental issues and fuel crisis.^[15,16] Biodiesel is considered as a promising alternative fuel compared with conventional petroleum diesel because the former is eco-friendly and promotes a positive life cycle–energy balance. Biodiesel has also a higher octane number and a higher flash point than diesel fuel, thereby providing better performance and safer use.^[17,18] Moreover, alkyl esters of fatty acids have been utilized as important ingredients in different uses, such as perfumes, flavors, cosmetics, food additives, lubricants for textiles, detergents, soaps, and plasticizers. Biodiesel is made from renewable resources and low-cost feedstocks, such as yellow greases, rendered animal fats, and trap greases that contain a high concentration of free fatty acids.^[19,20] Biodiesel is prepared through esterification of free fatty acids or the transesterification of triglycerides with methanol or other alcohols in the presence of acid or base catalysts.^[21–23] Industrial biodiesel production involves homogeneous base catalysis, which is correlated with a high production cost because this method encounters neutralization and separation problems.^[24] Base-catalyzed procedure suffers from several limitations of feedstock. For example, the free fatty acid content in the feedstock should be lower than 0.5 wt%, otherwise, biodiesel production will be badly hampered because of soap formation.^[24] On the other hand, concentrated sulfuric acid catalyzed esterification is basically a homogeneous processes, which is corrosive and critical for waste separation.^[25]

[a] Dr. S. K. Das, Prof. S. A. El-Safty

National Institute for Materials Science (NIMS)
1-2-1 Sengen, Tsukuba, Ibaraki 305-0047 (Japan)
Fax: (+81) 29-859-2501
E-mail: sherif.elsafty@nims.go.jp

[b] Prof. S. A. El-Safty

Graduate School for Advanced Science and Engineering, Waseda University
3-4-1 Okubo, Shinjuku-ku, Tokyo 169-8555 (Japan)
E-mail: sherif@aoni.waseda.jp

Supporting information for this article is available on the WWW under <http://dx.doi.org/10.1002/cctc.201300192>.

Solid acid catalysts are considered as suitable candidates for heterogeneous catalysis because of the limitations in homogeneous catalysis. Heterogeneous catalysis that involves the use of solid acid catalysts does not encounter corrosion issues and offers the usual advantages such as easy product isolation and catalyst reusability, thereby minimizing the loss of products during catalyst separation.^[26] To date, various solid acid catalysts such as zeolites,^[27,28] sulfated carbonized sugar,^[29,30] sulfated ZrO₂,^[31–33] sulfated silica–ZrO₂,^[34] Zr–PMOs,^[35] ion exchange resins and ionic liquid,^[36] zirconium phosphate/metal oxides,^[37] and organosulfonic acid functionalized mesoporous silica^[38,39] have been developed in biodiesel reaction. Zeolites are microporous solids and are no suitable candidates in biodiesel reaction because of the diffusion limitations of long-chain fatty acid molecules. Ion exchange resins are also not considered as potential candidates because of their low thermal stability. Solid acids usually catalyze the esterification reaction of fatty acids with methanol or with other small-chain alcohols at high temperatures ranging from 373 K to 453 K. Kiss et al. have displayed various interesting biodiesel catalysts, such as niobic acid, sulfated ZrO₂, sulfated titania, and sulfated tin oxide, and have revealed that sulfated ZrO₂ is the most active in this aspect.^[17,28] Another sulfated-ZrO₂-anchored mesoporous silica catalyst has also been reported by Chen et al. for the heterogeneous catalysis of the esterification of long-chain fatty acids.^[34] Myristic acid has been esterified with short-chain alcohols by using sulfated ZrO₂.^[31] Rebeca et al. showed that Zr-loaded mesoporous organic–inorganic hybrid silica catalyzed the biodiesel production through esterification/trans-esterification of free fatty acids in the feedstock.^[35] Thus, we have also developed zirconium oxophosphates for the heterogeneous catalysis of the esterification reaction of different long-chain fatty acids with methanol.^[40] Moreover, studies have shown that researchers are extremely interested in developing heterogeneous recyclable catalysts in biofuel preparation, and that the invention of suitable green catalysts is a big challenge today.

In this context, we herein present the development of new mesoscopically assembled zirconium nanostructures (MAsZrNPs) by using premade NPs as a framework building block through the use of a template as a fastening agent in an acidic aqueous medium. The porous frameworks were generated by removing the fastening template molecules and internal rearrangement of NPs at high-temperature calcination. The highly crystalline characteristic of the NPs effectively sustained the local strain during mesophase formation. The pore walls of the materials were composed of individual NPs, which provided high structural stability at high temperatures and in harsh chemical reactions. The utilization of premade NPs minimized the possibility of increased NP size during the entire porous-structure creation, and provided a higher surface area than if bulk NPs were used. The sulfated matrix was used as an efficient heterogeneous solid acid catalyst in the biodiesel reaction, such as in the conversion of long-chain fatty acids to their corresponding esters in mild reaction conditions. A high surface area facilitates the integration of the sulfate functionality and an open framework structure provides easy access to

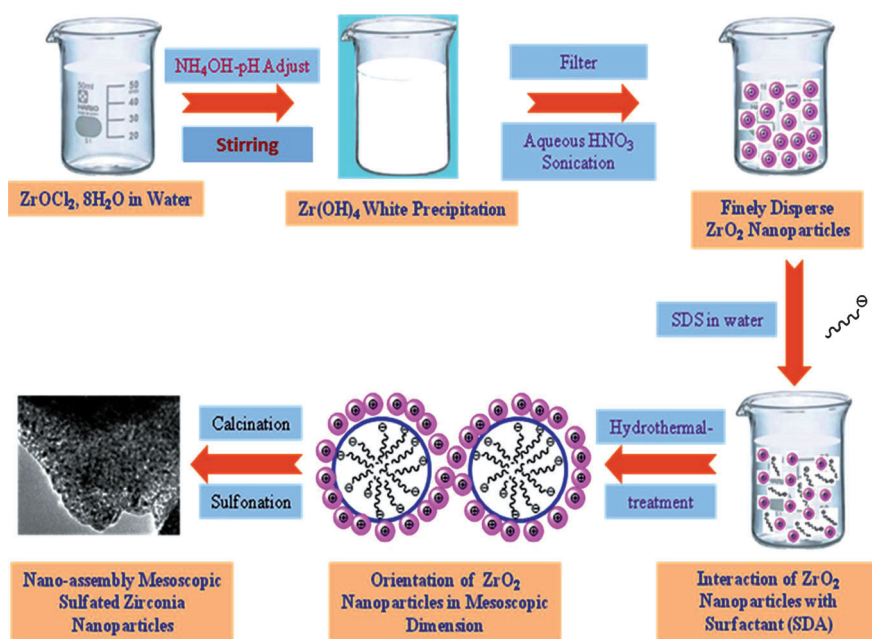
the active sites in the chemical reactions. Large pore sizes favor the diffusion of large-size fatty acid molecules. With the presence of strong acid sites, the biodiesel reaction rate significantly accelerates in optimal reaction conditions.^[40,41] The sulfated MAsZrNPs (MAsSZrNPs) functioned as heterogeneous and recyclable catalysts in the biodiesel reaction, and the maximum biodiesel yield was approximately 100%. To our knowledge, the fabrication of such mesoporous nanoassemblies by using premade monodisperse NPs with a high surface area and sodium dodecyl sulfate (SDS) as a fastening agent in the hydrothermal method and their utilization as heterogeneous solid acid catalysts in biodiesel reactions were not explored until now. The mesoporous nanoassemblies provided efficient catalytic reusability in the biodiesel reaction with negligible loss of activity.

Results and Discussion

Fabrication of MAsZrNPs biodiesel catalysts

The development of new MAsZrNPs by using premade NPs as a framework building block through the use of a template as a fastening agent (Scheme 1) is highly challenging. The entire synthetic process involved the following: 1) Preparation of a sol of highly disperse and very small ZrO₂ NPs and their utilization as framework building units. 2) Fastening of ZrO₂ NPs with a template molecule, because the pH of the solution (pH ≈ 1) was below the point of zero charge (4–6),^[14] thus, positively charged ZrO₂ NPs interacted with the negative head group of the anionic structure-directing agent (SDS) through electrostatic interaction, and a mesoscopic assembly architecture was generated. 3) Generation of porous frameworks through the removal of the fastening template molecules and the internal rearrangement of NPs by high-temperature calcination; the highly crystalline nature of NPs effectively sustained local strain, which was owing to the mesophase formation.

The main advantages of these frameworks are as follows: 1) individual NPs compose the pore walls of the matrix and provide a high structural stability at high temperatures and in harsh chemical reaction conditions. 2) Premade NPs minimize the possibility of NP size increase throughout the porous framework construction. 3) The special arrangement of NPs generates a porous framework with a higher surface area than that of bulk NPs. Hence, these frameworks are useful catalysts because they have plenty of accessible active sites. Moreover, large pores and an open framework structure facilitate the diffusion of large fatty acid molecules. NP morphology and crystallinity were confirmed by high-resolution TEM (HRTEM), selected-area electron diffraction (SAED) analysis (Figure 1), and wide-angle powder X-ray diffraction (PXRD) analysis (Figure 2B). The small-angle PXRD results of calcined sulfated materials suggested that the structure was retained and the mesoscale was porous (Figure 2A and Figure S1A in the Supporting Information). The electron diffraction spectroscopy results for chemical surface analysis revealed the successful integration of the sulfate functionality (Figure S2). The main advantages of the materials for catalysis were as follows: 1) They exhib-



Scheme 1. The formation of nanoassembly MASzrNPs through the hydrothermal method by using an anionic structure-directing agent (SDS) as a fastening agent.

ited a high surface area that integrated the sulfate functionality and an open-framework structure that provided easy access to the active sites during the chemical reaction. 2) The sulfated MASzrNPs functioned as heterogeneous and recyclable catalysts in the biodiesel reaction during the transformation of long-chain free fatty acids into their corresponding esters. The obtained maximum biodiesel yield was approximately 100%.

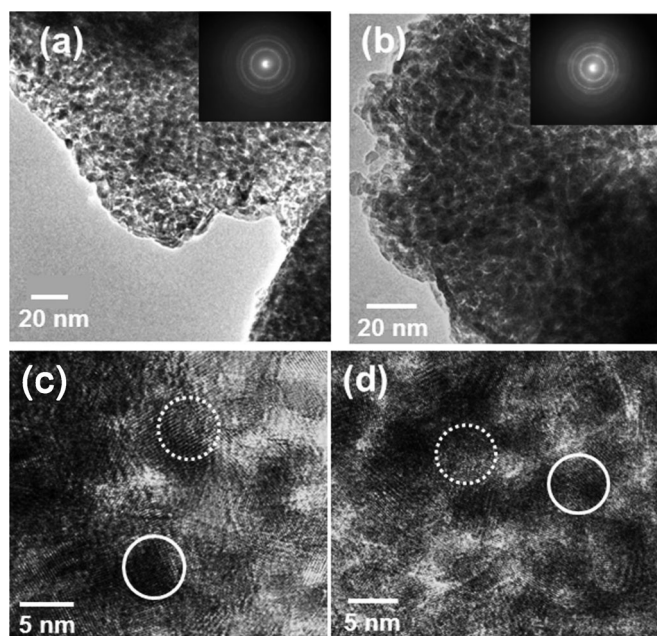


Figure 1. TEM images of calcined samples a) MASzrNPs-1 and b) MASzrNPs-2 seen through the direction perpendicular to the pore axis. The corresponding SAED patterns are shown in the insets, respectively. HRTEM images of the calcined materials: c) MASzrNPs-1 and d) MASzrNPs-2.

3) The heterogeneous catalytic activity of MASzrNPs was excellent, which could be attributed to the large surface area, the presence of ample acidic sites located at the surface of the matrix, and its stability towards harsh chemical reaction conditions. Two NH_3 desorption peaks were assigned at 278.9 and 639 K for MASzrNPs (Figure S3). Compared to the desorption peak of recently prepared sulfated zirconia at 635 K,^[14] the peak of MASzrNPs appeared at much higher temperature. These findings revealed that the fabrication strategy of sulfonated nanoassembled zirconia led to a strong binding of ammonia to highly acidic sites. 4) The catalyst exhibited a negligible loss of activity in the catalytic cycles.

This concept can, therefore, be utilized to design and synthesize other mesoscopic-assembly materials. These materials may also be of great importance to other acid-catalyzed reactions.

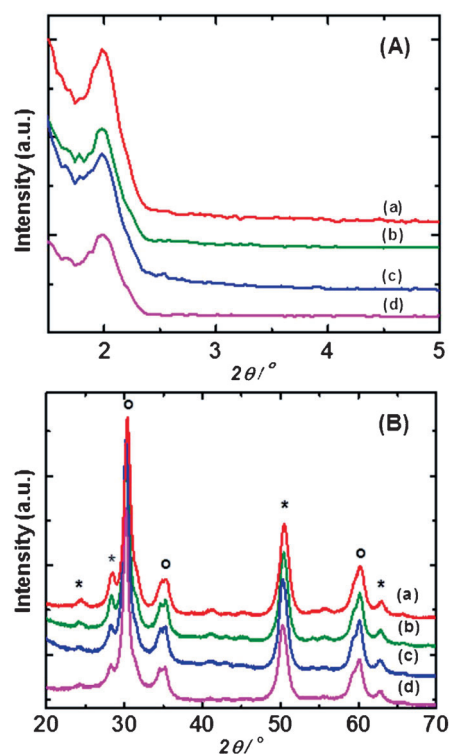


Figure 2. A) Small-angle XRD patterns of sulfated samples: a) MASzrNPs-1, b) MASzrNPs-2, c) MASzrNPs-3, and d) MASzrNPs-4. B) Wide-angle XRD patterns of sulfated samples: a) MASzrNPs-1, b) MASzrNPs-2, c) MASzrNPs-3, and d) MASzrNPs-4; (*) monoclinic phase, (o) tetragonal phase.

High-resolution TEM analysis

Representative TEM images of the calcined MASzrNPs are shown in Figure 1a,b. In these images, low-electron-density spots (pores) were observed throughout the respective specimens, and particles of sizes of approximately 7.0–9.0 nm were arranged in a mesoscopic order. Interparticle pores, as seen in these images, varied from 4.0 to 6.0 nm in length. The SAED analysis results (insets in Figure 1a and b) of the mesoporous MASzrNPs confirmed that the pore walls of our studied materials were made up of nanocrystalline oxides, which exhibited characteristic diffuse electron diffraction rings. These well-resolved diffraction rings were attributed to the polycrystalline nature of NPs.^[13,14] HRTEM images revealed the orientation of the NPs within the pore walls and several nanocrystallites with well resolved lattice planes, as shown in Figure 1c and d. Here, the marked white portion within the dashed circles were the pores, whereas the marked black portion within the solid circles were the observed NPs. The average pore diameters measured from this micrograph were consistent with the pore size distribution derived by using the nonlocal density functional theory (NLDFT) method from the N₂ adsorption/desorption isotherms, as shown in Figures 3 and 4.

Powder X-ray diffraction

The small-angle PXRD patterns for the calcined MASzrNPs are shown in Figure 2A and Figure S1A, respectively. Both types of materials exhibited a single broad peak in their respective

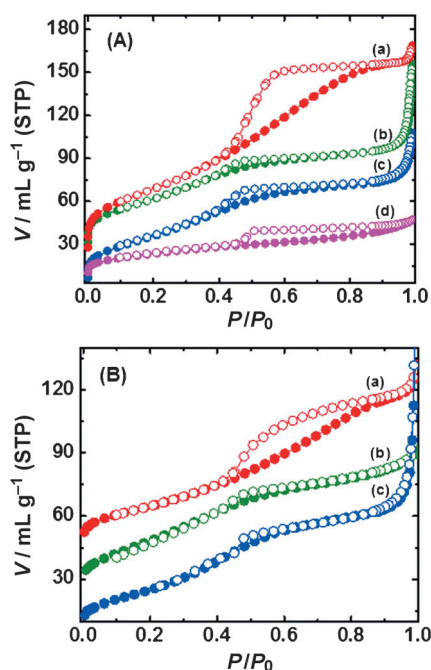


Figure 3. N₂ adsorption/desorption isotherms of A) calcined samples a) MASzrNPs-1, b) MASzrNPs-2, c) MASzrNPs-3, and d) MASzrNPs-4; B) calcined mesoporous sulfated samples a) MASzrNPs-1, b) MASzrNPs-2, and c) MASzrNPs-3 measured at 77 K. Adsorption points are marked by filled circles and desorption points by empty circles.

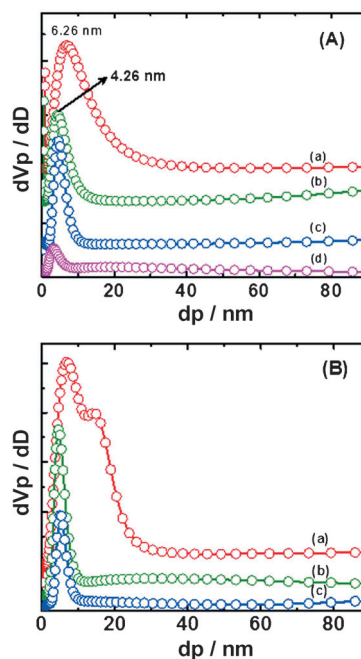


Figure 4. NLDFT pore size distribution of A) calcined samples: a) MASzrNPs-1, b) MASzrNPs-2, c) MASzrNPs-3, and d) MASzrNPs-4; B) calcined sulfated samples a) MASzrNPs-1, b) MASzrNPs-2, and c) MASzrNPs-3. V_p = pore volume, d_p = pore diameter.

small-angle PXRD patterns. This result suggests that the NPs were arranged more or less disorderly in these materials, as shown in the TEM images (Figure 1).^[14] The calcined MASzrNPs exhibited a diffraction peak at ca. 2.00° (2 θ), which indicates a d spacing of ca. 4.41 nm, whereas in MASzrNPs, this diffraction peak slightly shifted to approximately 1.95°, and the corresponding d spacing was approximately 4.52 nm. The XRD results were consistent with the TEM micrographs and the N₂ sorption analysis results. The small-angle PXRD results demonstrate the existence of mesoporosity in both types of materials, and during high-temperature calcinations, individual NPs rearranged to create mesoporosity. The highly crystalline nature of the materials effectively sustained the local strain during mesophase formation.^[4,11]

The wide-angle PXRD patterns of the calcined MASzrNPs are shown in Figure 2B and Figure S1B, respectively. The XRD results for both types of materials exhibited a mixture of well-resolved characteristic of monoclinic and tetragonal phases of individual ZrO₂ NPs.^[13,42–44] Calcined MASzrNPs possessed a tetragonal phase, which is its major characteristic (Figure 2B). After sulfate integration, the monoclinic phase became more prominent, as observed in the Figure S1B. Thus, integrated sulfate ions had a strong influence on phase modification. Sulfate ions converted the metastable tetragonal phase to its more thermodynamically stable monoclinic phase.^[42] In the current research, the particle sizes of NPs were calculated by using the Scherrer equation. The estimated particle sizes varied from 7.0 to 9.0 nm (see the Supporting Information). These results were in agreement with the TEM image analysis results (Figure 1).

N₂ sorption studies

N₂ sorption studies are important to determine the porous nature of the materials. N₂ sorption measurements were conducted on the calcined and sulfated mesoporous MASzrNPs at 77 K, and the type-IV adsorption-desorption isotherm exhibited a small hysteresis loop, as shown in Figure 3 A and B, respectively. Type-IV isotherms are characteristic of mesoporous materials, and desorption hysteresis results suggested the existence of large mesopores in the sample.^[45] This hysteresis was an intermediate between typical H₂- and H₄-type hysteresis loops in a relative pressure range P/P_0 from 0.40 to 0.9. This result suggested that large mesopores with cage-like pore structures were connected by windows with small sizes.^[10,46] This characteristic is typical of capillary condensation within uniform pores. In the current research, the BET surface area, average pore diameter and pore volume for the calcined and sulfated mesoporous MASzrNPs are shown in Table 1 (en-

Table 1. Physico-chemical properties of mesoscopic-assembly zirconia and sulfated zirconia nanoparticles.					
Entry	Sample type	Surface area [m ² g ⁻¹]	Pore width [nm]	Pore volume [cm ³ g ⁻¹]	Particle size [nm]
1	MAsZrNPs-1	183	6.26	0.272	7.63
2	MAsZrNPs-2	142	4.26	0.265	8.13
3	MAsZrNPs-3	139	4.24	0.207	8.34
4	MAsZrNPs-4	67	4.02	0.082	8.69
5	MAsSZrNPs-1	93	6.87/14.20	0.160	7.94
6	MAsSZrNPs-2	103	4.59	0.114	7.21
7	MAsSZrNPs-3	98	4.87	0.272	8.21

tries 1–4 for the calcined MASzrNPs and entries 4–7 for the sulfated MASzrNPs). The BET surface area of the calcined MASzrNPs-1, MASzrNPs-2, MASzrNPs-3, and MASzrNPs-4 were 183, 142, 139, and 67 m² g⁻¹, respectively. The surface area of the sulfated MASzrNPs-1, MASzrNPs-2, and MASzrNPs-3 were 93, 103, and 98 m² g⁻¹, respectively. The pore volumes of the corresponding calcined materials decreased after the incorporation of the sulfate group, as shown in Table 1 (entries 4–7). Thus, the surface areas as well as the pore volumes of the calcined matrices decreased upon sulfate integration, which can be attributed to the dispersion of sulfate groups on the surface of the porous framework. Moreover, a kind of pore blocking can also occur.^[26] The pore sizes of MASzrNPs, as shown in Figure 4A and estimated by employing the NLDFT method, were in agreement with the pore widths obtained from TEM images (Figure 1) and XRD analysis results (Figure 2A and Figure S1B).

UV/Vis diffuse reflectance spectra

UV/Vis spectroscopy was performed to characterize the optical properties of the ZrO₂ nanocrystals, which contained pore walls of the mesoporous self-assembly architecture. In Figure 5 and Figure S3, UV/Vis diffuse reflectance spectra of the calcined and sulfated mesoporous MASzrNPs are shown, respectively. The spectral features of these materials were almost

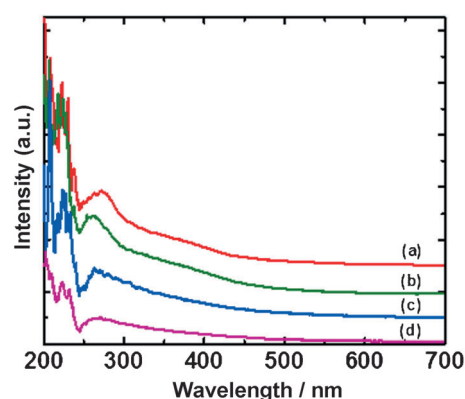


Figure 5. UV/Vis reflectance spectra of calcined samples: a) MASzrNPs-1, b) MASzrNPs-2, c) MASzrNPs-3, and d) MASzrNPs-4.

identical. The absorption band at approximately 208 nm appeared because of the ligand-to-metal charge-transfer transition (O²⁻ → Zr⁴⁺). Furthermore, a weak broad band was observed in the region from 224 to 230 nm. This result can be attributed to the presence of Zr–O–Zr linkages in the framework.^[34] The UV absorption edge wavelength is very sensitive to the particle size of semiconductor nanocrystals.^[47,48] For NPs (< 10 nm), the band gap energy increases with decreasing crystal size, and the absorption edge of the interband transition is blueshifted. Such blueshifts of the interband transition energy (band gap) were clearly observed in the UV region of the diffuse reflectance spectra for very small ZrO₂ nanocrystals because of the appearance of an additional peak in the region from 270 to 290 nm.^[14] This spectroscopic result suggested that ZrO₂ nanocrystals compose the pore walls of the mesoporous MASzrNPs structure. However, unlike conventional mesoporous materials with a continuous pore wall, the pore walls of MASzrNP materials can be considered as composed of discrete nanodomains separated by voids.

FTIR spectroscopy

The FTIR spectra of the calcined and sulfated MASzrNPs are shown in Figure 6. The absence of bands at approximately $\nu = 2854$ and approximately 2925 cm⁻¹ in these samples, which are ascribed to the symmetric and asymmetric vibrations of the C–H groups, indicated the complete removal of surfactant molecules after calcination. The broad bands at approximately $\nu = 3000$ to 3600 and 1620 cm⁻¹ were attributed to the asymmetric OH stretching and vibration bending of the adsorbed water molecule, respectively.^[48] The spectral feature ranging from $\nu = 1400$ to 900 cm⁻¹ was very important in characterizing the presence of sulfate moieties in MASzrNPs, and all MASzrNP materials exhibited almost similar spectral features. The observed band at $\nu = 960$ cm⁻¹ indicated S–O symmetric stretching, whereas other bands at higher frequencies, such as $\nu = 1033$, 1069 , 1128 , and 1236 cm⁻¹, were attributed to S–O asymmetric stretching.^[49] Furthermore, the presence of another band at $\nu = 1380$ cm⁻¹ indicated the asymmetric stretching of S=O, which was bonded to the ZrO₂ NPs.^[50] From the spectral data, MASzrNPs-2 had numerous intense bands in the sulfate

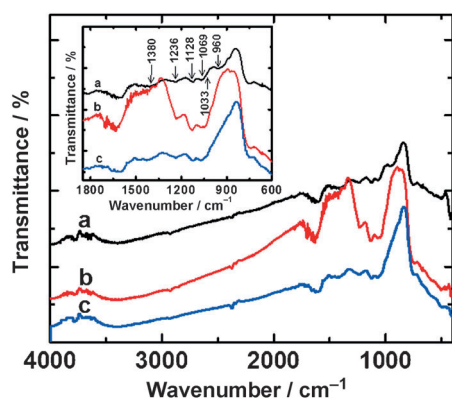


Figure 6. FTIR spectra of the sulfated samples: a) MASzrNPs-1, b) MASzrNPs-2, and c) MASzrNPs-3. In the inset, the corresponding FTIR spectra ranging from $\nu = 1800$ to 800 cm^{-1} are shown.

region of asymmetric stretching, and this result may explain the higher catalytic efficiency of MASzrNPs-2 in biodiesel reaction (acid-catalyzed reaction) than that of the other two samples. Thus, this spectral investigation described the integration of sulfate moieties into the ZrO_2 NPs. The partial ionic nature of the S–O bonds was responsible for the strong Brønsted acidity of the sulfate-modified ZrO_2 NPs.^[51] The high surface area of the mesoporous MASzrNPs facilitated the integration of the sulfate functionality to a suitable extent within its framework; hence, acid-catalyzed reactions were accelerated.

Catalytic reaction

The catalytic performance of sulfated MASzrNPs in biodiesel synthesis was investigated through the esterification of different long-chain fatty acids with methanol. In this study, methanol was used as a reactant as well as a solvent for the liquid phase. In all cases, only the methyl ester of the corresponding fatty acid was formed as a product with 100% selectivity. The results of the catalytic activities of MASzrNPs are given in Table 2. In view of their good catalytic activity, a sulfate-loaded MASzrNPs-2 catalyst was considered, at a typical loading of 2.14 wt% with respect to fatty acid (oleic acid), to obtain a maximum yield of 100% (Zr/S molar ratio of 16.54)

with a turnover number (TON) of 18.53 at 323 K after 8 h of reaction time (entry 13). If the fatty acid (oleic acid) to alcohol (methanol) molar ratio was changed to 10, the yield and TON were not significantly affected (entry 15). TON calculation was performed based on chemical analysis, as shown in the Supporting Information (Figure S2). A decrease in Zr/S molar ratio to 15.13 (MASzrNPs-1), which corresponded to an increase in the integrated sulfate group amount in the matrix, lowered the yield to 77% and reduced the TON to 14.26 (Table 2, entry 14). MASzrNPs-1 at 3 wt% resulted in a lauric acid methyl ester yield of 89% with a TON of 17.11 (entry 8), whereas 6 wt% of the respective catalyst resulted in a yield of 91%. The increase was small, but the TON decreased to 8.75 (entry 9) without changing other reaction parameters.

To study temperature effects, lauric acid was used as a reference. For example, the temperature was lowered to 283 K in the case of MASzrNPs-2, which resulted in a decrease of the yield to 38% and TON to 7.04 (Table 2, entry 17), whereas increasing the temperature to 303 K resulted in an increase of the yield to 86% and the TON to 15.93 (entry 6). Increasing the temperature of the reaction to 323 K increased the yield to 96% and the TON to 17.78 (entry 10). If the system was catalyzed by a nonsulfated MASzrNPs-1 catalyst, the yield de-

Table 2. Biodiesel reaction of different long chain fatty acids with methanol catalyzed by mesoscopic assembly zirconia and sulfated zirconia nanoparticles.^[a]

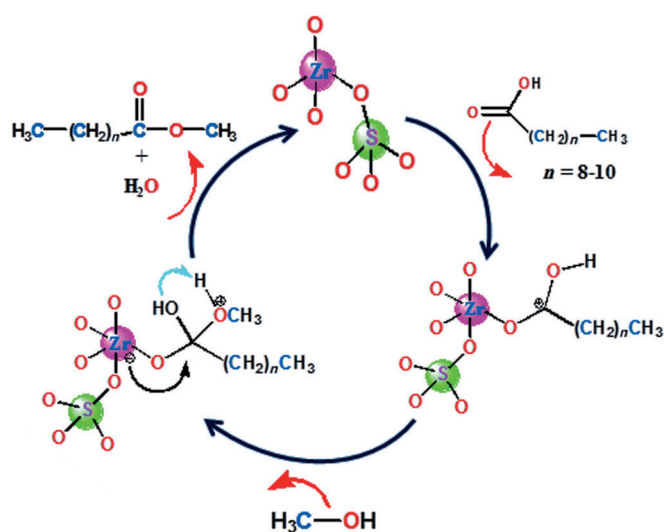
Entry	Catalyst type	Fatty acid	Alcohol/acid molar ratio	Catalyst [wt %]	Temperature [K]	Yield [%]	TON ^[b]
1	MASzrNP-1	decanoic acid	10	3.48	303	57	10.96
2	MASzrNP-2	decanoic acid	10	3.48	303	86	15.93
3	MASzrNP-1	decanoic acid	10	3.48	323	81	15.58
4	MASzrNP-2	decanoic acid	10	3.48	323	97	17.96
5	MASzrNP-1	lauric acid	10	3.00	303	76	14.61
6	MASzrNP-2	lauric acid	10	3.00	303	86	15.93
7	MASzrNP-3	lauric acid	10	3.00	303	42	7.78
8	MASzrNP-1	lauric acid	10	3.00	323	89	17.11
9 ^[c]	MASzrNP-1	lauric acid	10	6.00	323	91	8.75
10	MASzrNP-2	lauric acid	10	3.00	323	96	17.78
11 ^[d]	MASzrNP-2	lauric acid	20	3.00	303	93	17.22
12 ^[e]	MASzrNP-2	lauric acid	20	3.00	323	95	17.59
13	MASzrNP-2	oleic acid	20	2.14	323	100	18.53
14	MASzrNP-1	oleic acid	10	2.14	323	77	14.26
15	MASzrNP-2	oleic acid	10	2.14	323	99	18.34
16	MASzrNP-3	oleic acid	10	2.14	323	72	13.33
17 ^[f]	MASzrNP-2	lauric acid	10	3.00	283	38	7.04
18 ^[g]	MASzrNP-1	lauric acid	10	3.00	323	21	4.32
19 ^[h]	–	lauric acid	10	–	323	4	–

[a] Conditions, unless stated otherwise: The esterification of long-chain fatty acids with methanol was performed with a mole ratio of fatty acid/methanol of 1:10 and 1:20 (entries 11–13). The catalyst (≈ 30 mg) and fatty acid (5 mmol) were used for each set of the reaction. [b] TON = moles of product or yield/mole of active sites (e.g., disperse Zr sites) of the catalyst. [c] Esterification of lauric acid with double amount of the catalyst (60 mg) at 323 K. [d] Esterification of lauric acid with a mole ratio of fatty acid/methanol of 1:20 at 303 K. [e] Esterification of lauric acid with a mole ratio of fatty acid/methanol of 1:20 at 323 K. [f] Esterification of lauric acid at 283 K. [g] Esterification of lauric acid in the presence of unsulfated MASzrNPs-1 catalyst. [h] Esterification of the lauric acid in the absence of a catalyst. In each case, the product selectivity was 100%, and the conversion of all the products was measured after 8 h.

creased to 21% and the TON to 4.32 (entry 18) during lauric acid esterification at 323 K for 8 h. Thus, sulfate functionalization is important for the efficient biodiesel reaction of different fatty acids with methanol in mild reaction conditions. Blank experiments confirmed that fatty acid esterification did not occur considerably in the absence of the MASZrNPs catalysts (entry 19). From the catalytic results, the MASZrNPs-2 catalyst provided the highest efficiency in biodiesel reaction compared with the other two materials, and also provided the maximum yield of oleic acid.

Methanol was used in a large excess relative to the fatty acids because it functions as a reactant as well as a solvent in this type of reaction. The use of a small amount of methanol (methanol/fatty acid molar ratio 1:1) relative to the fatty acid in the respective biodiesel reaction provided a viscous mixture of the reactant and product, which was difficult to separate.^[23] Excess methanol helps dissolve the fatty acid; thus, other solvents are not needed. Methanol also facilitates the conversion to the desired product. Excess methanol used in the reaction can be reused in the next run. The boiling point of methanol is relatively low; thus, the separation of excess methanol from the product mixture is not difficult. Particularly, the isolation of the biofuel product becomes much easier if methanol is used in excess in the reaction mixture.

The use of surface-sulfate-modified zirconia NPs was vital in the esterification reaction of fatty acids, as shown in Scheme 2. Studies have shown that sulfated ZrO₂ has a strong Brønsted acidity, and usually favors this type of reaction.^[14,22,34,40,51,52] In the reaction, the long-chain fatty acid is dissolved in methanol in the presence of a catalyst (MASZrNPs), and the polar carboxylic group (–COOH) of the fatty acid is adsorbed to the catalytic active sites on the surface of the material. Large pores facilitate the diffusion of bulky-sized fatty acid molecules through the pore interior, and a high surface area provides plenty of active sites for the reaction. The presence of sulfonic acid on the surface of the catalyst leads to a slight positive



Scheme 2. The catalytic cycle during the biodiesel reaction of long-chain fatty acids with methanol by using calcined sulfated MASZrNPs.

charge (δ^+) on the carbonyl carbon of the reacting fatty acid through the protonation of the adjacent oxygen atom. Consequently, the nucleophilic methanol (MeOH) molecule attacks the carbonyl carbon, because the latter has a very high electrophilicity. After internal rearrangement, the methyl ester of the corresponding fatty acid and water are formed in the reaction. In the end, the final products are easily desorbed from the surface of the catalyst to the bulk reaction medium because the polarity of the esterified products is lower compared to that of the reactant (free fatty acids). In general, the MASZrNPs catalysts exhibited a catalytic activity significantly higher than that of other heterogeneous or homogeneous acid and base catalysts,^[17,25,28,34,40,52,53] which also require intensive design and experimental conditions in such biodiesel catalytic reactions (Table 3).

Table 3. Comparative study of reported biodiesel heterogeneous catalysts with our studied materials.^[a]

Entry	Sample	Amount [wt %]	Fatty acid/alcohol molar ratio	Temp [K]	Time [h]	Conv [%]	Ref.
1	SZ	1	1	403	2	40	[17]
2	SiO ₂ -SZ	5	10	361	6	90	[34]
3	porous ZrP	5	10	338	24	89	[40]
4	SBA-15-SO ₃ H	10	20	358	3	84	[39]
5	HZnPS-1	5	10	298	24	95	[23]
6	H ₂ SO ₄	1	1	403	1	96	[25,28]
7	MASZrNPs-1	2.14	10	323	8	77	this work
8	MASZrNPs-2	2.14	10	323	8	99	this work

[a] Sulfated zirconia = SZ.

The stability of the MASZrNPs catalysts as well as the heterogeneous nature of the catalysis was tested by recycling the catalyst. The hot filtration of a MASZrNPs-2 catalyst solution in optimized reaction conditions allowed the separation of the solid catalyst, which was then reused with fresh reagents in the same reaction conditions. No loss of catalytic activity was observed. Moreover, the filtered solution was immediately used for catalysis upon the addition of methanol, and the catalyst was not active in increasing fatty acid esterification. These results indicated that during the reaction, no appreciable catalyst leaching occurred, and the reaction was essentially heterogeneous. The activity of a regenerated catalyst was inspected upon separation of the solid catalyst from a reaction mixture through filtration, several times washing with methanol and anhydrous acetone, and drying in an oven at 373 K overnight. The catalyst was subsequently activated at 473 K for 4 h under air flow, and was then utilized for the above reaction. The same procedure was repeated five times with negligible loss of activity, as shown in Figure 7. A marginal loss of catalytic activity of the sulfated catalyst in the biodiesel reaction was observed after several reuses/cycles. This loss of catalytic activity was possibly attributable to 1) formation of water molecules during the esterification reaction, which assisted in the deactivation of active sites. 2) Leaching of the sulfate sites to a negligible extent from the catalyst in the polar alcohol medium

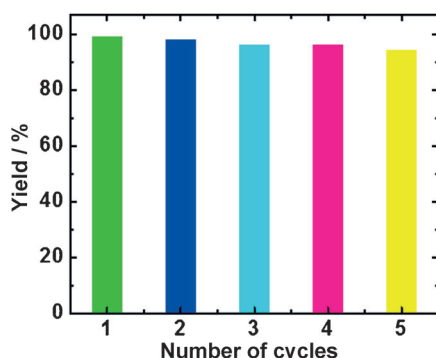


Figure 7. Product yields in various runs, upon catalyst recycling for biodiesel reaction of long-chain fatty acid with methanol by using sulfated MASZrNPs-2 catalyst. Oleic acid was used as the reference fatty acid.

during the course of reaction. Thus, the sulfated mesoporous MASZrNPs described herein have a great potential to be used as a stable and highly active recyclable solid acid catalyst in biofuel preparation.

Conclusions

In conclusion, we presented a simple and convenient synthetic method for the fabrication of MASZrNPs by using very fine monodisperse ZrO₂ nanoparticles (NPs) through the template pathway in an acidic aqueous medium. The self-assembly process was explained by the constructive charge interactions among NPs with micellar aggregates. The self-assembly methodology, that is, NP/surfactant fastening interactions, is general and could open up a new window to other types of mesoscopic assembly of semiconductor NP systems, as well as oxometalate cations and anions. High-resolution TEM and N₂ sorption studies revealed the formation of large mesopores through the arrangement of NPs. The integration of sulfate made this material an excellent heterogeneous biodiesel catalyst for the effective conversion of long-chain fatty acids to their methyl esters (yield ≈ 100%), as shown in Table 3. The excellent heterogeneous catalytic activity and stability could be attributed to the high surface area and acidic sites located on the surface of the MASZrNPs catalysts. Moreover, this material provided efficient reusability as a catalyst in the designed reaction with negligible loss of activity, a feature of high importance in the heterogeneous catalysis in the face of fuel crisis and environmental concerns. Catalytic significance also confers its paramount importance to other acid-catalyzed reactions.

Experimental Section

Characterization techniques

PXRD analyses of the samples were performed by using a D8 Advance Bruker AXS diffractometer operated at 18 kW and calibrated with a standard silicon sample. A Ni-filtered CuK_α (λ = 0.15406 nm) radiation was used. TEM images and SAED patterns were obtained by using a JEOL JEM model 2100F microscope operated at 200 kV. TEM images were obtained by using a CCD camera. SAED patterns were obtained by using an image-plate magazine. The elemental

composition of the sulfated mesoporous MASZrNPs were estimated through SEM (field-emission scanning electron microscope, JEOL model 6500). A JEOL JEM 6500 field-emission scanning electron microscope attached to an energy-dispersive spectroscopy and operated at 20 keV was used to determine the elemental composition of the sulfated mesoporous MASZrNPs. The nitrogen adsorption/desorption isotherms of the samples were obtained by using a BELSORP36 analyzer (JP. BEL Co., Ltd.) at 77 K. Prior to the gas adsorption/desorption measurements, all samples were degassed at 473 K for 4 h in a high-powered vacuum. The BET specific surface area was computed by using the adsorption data at a relative pressure range of P/P_0 from 0.05 to 0.30. The pore size distribution was derived from the adsorption isotherms by using NLDFT. The total pore volume was estimated from the amounts adsorbed at a $P/P_0 = 0.99$. The NH₃ temperature-programmed desorption (NH₃-TPD) measurements were conducted on an Autochem 2910 instrument, and a thermal conductivity detector was used for continuous monitoring of desorbed ammonia. Prior to TPD analysis, the sample was pretreated at 400 °C for 1 h in a flow of ultra-pure helium gas (40 mL min⁻¹), and the sample was cooled to 100 °C in the flow of ultra-pure helium gas. The pretreated sample was then saturated with 10% anhydrous ammonia gas (balance He, 60 mL min⁻¹) at 50 °C for 2 h and subsequently flushed with He (60 mL min⁻¹) at 100 °C for 2 h to remove the physisorbed ammonia. The heating rate of the TPD measurements, ranging from 100 °C to 700 °C, was 10 °C min⁻¹. ¹H NMR experiments were performed on a Bruker Avance DRX 600 MHz (UltraShield Plus Magnet) NMR spectrometer at ambient temperature. The FTIR spectra of these samples were obtained by using an IR Prestige-21 spectrophotometer from Shimadzu. The UV/Vis diffuse reflectance spectra were obtained by using a Shimadzu 3150 spectrophotometer.

Chemicals

Anionic structure-directing agent CH₃(CH₂)₁₁OSO₃Na (SDS) and different fatty acids, such as decanoic acid, lauric acid, and oleic acid, and methanol were purchased from Sigma-Aldrich. Zirconyl chloride (ZrOCl₂·8H₂O), ammonia (NH₃, 28%, aqueous solution), and nitric acid (HNO₃, 60%) were obtained from Wako Chemicals. Chloroform-d (CDCl₃, 0.05% TMS (v/v) + 99.8 atom% D) was received from Isotec. All these chemicals were used without further purification.

Synthesis

The synthesis involved two steps: 1) the synthesis of ZrO₂ NPs and 2) the fabrication of a mesoscopic nanoassembly architecture.

Preparation of a sol of uniform monodisperse ZrO₂ NPs: ZrO₂ NPs were prepared by using suitable modification of previous work published elsewhere.^[54] Briefly, in a typical synthesis, zirconyl chloride (ZrOCl₂·8H₂O, 3.22 g, 10 mmol) was dissolved in distilled water (100 mL). The pH of the solution was rapidly adjusted to approximately 10 by using an NH₃ solution to form hydroxide precipitates. The precipitate was filtered and thoroughly washed with an excess of distilled water to remove NH₃ and chloride. The precipitate was then transferred to an aqueous acidic (HNO₃) solution and was sonicated until a transparent NPs sol was generated. The final pH of the solution was < 1, and the generated particles remained highly dispersible without sedimentation for a prolonged period.

Preparation of MASZrNPs: MASZrNPs were constructed by using premade ZrO₂ NPs as building blocks. In the synthetic procedure, premade ZrO₂ NPs (1 mmol) were added to SDS solution (0.320 g,

1.1 mmol) solution in water (80 mL) at vigorous stirring at ambient temperature. The solution was stirred for 2 h. This solution was then stirred further in an oil bath at 353 K for 3 h and slowly cooled down to RT. The self-assembled NPs were separated through centrifugation and dried in vacuum. Calcination was performed on the as-synthesized material by slowly increasing the temperature to 873 K (1 K min⁻¹ ramping rate) followed by heating at 873 K for 5 h in the presence of air to obtain template-free MASZrNPs. This sample was designated as NAsZrNPs-1.

The other three materials were prepared by varying the molar ratio of the precursors, such as $XZrO_2/YSDS/ZH_2O$. In all these cases $X=1$, and only Y and Z were varied. The four sets of variation were $Y=0.56$, $Z=2224$; $Y=0.28$, $Z=1112$; and $Y=0.14$ and $Z=556$. The sample abbreviations were NAsZrNPs-2, NAsZrNPs-3, and NAsZrNPs-4, respectively.

Preparation of MASZrNPs: The sulfation of ZrO₂ NPs was performed by treating the above-prepared calcined MASZrNPs material (1.0 g) with 1 N sulfuric acid aqueous solution (15 mL), followed by calcination in air at 833 K (2 K min⁻¹ ramping rate) for 2 h.

Catalytic reactions

The catalytic biodiesel reactions were performed in a round-bottom flask fitted with a water condenser and placed in a temperature-controlled oil bath with a magnetic stirrer. In the biodiesel reaction, different long-chain fatty acids are esterified with a low-molecular weight alcohol, such as methanol. In a typical batch, fatty acid (5 mmol) was dissolved in a suitable amount of methanol, and an amount of catalyst was added. The solution was then placed in an oil bath at a specified temperature and was stirred for 8 h. After completion of the reaction, the product was collected by separating the solid catalyst through filtration. The methanol solvent was then separated from the product mixture (filtrate) by vacuum evaporation. We varied the catalyst amount from 3.5 wt% to 5.8 wt% depending on the substrate, and we varied the temperature from 283 K to 323 K. Moreover, we varied the molar ratios of the fatty acids and methanol from 1:10 to 1:20. Methanol was used in large excess because it was used as a reactant as well as a solvent. The product yield was calculated by NMR spectroscopy.

Reuse of the catalyst

At the end of the reaction, the catalyst was separated from the reaction mixture through filtration. The catalyst was thoroughly washed with methanol and *n*-hexane or acetone for several times to remove both nonpolar and polar compounds that were adsorbed on the surface and in the interior pores of the catalysts. After washing, the catalysts were activated by heating overnight at 373 K, followed by 473 K for 4 h, and then used again for the same reaction in identical reaction conditions. The whole process was repeated five times for recycling experiments. Negligible loss of the catalytic activity was observed. Catalyst reusability was tested by using oleic acid and MASZrNPs-2 as the reference fatty acid and catalyst, respectively (Figure 7). The product yields for various cycles (Figure 7) were very consistent, suggesting high catalytic efficiency and stability of MASZrNPs in the biodiesel synthesis reactions.

Keywords: fatty acids · heterogeneous catalysis · mesoporous materials · nanostructures · zirconium

- [1] a) G. Liu, Y. Zhao, C. Sun, F. Li, G. Q. Lu, H. M. Cheng, *Angew. Chem.* **2008**, *120*, 4592–4596; *Angew. Chem. Int. Ed.* **2008**, *47*, 4516–4520; b) W. Wei, C. Yu, Q. Zhao, G. Li, Y. Wan, *Chem. Eur. J.* **2013**, *19*, 566–577.
- [2] a) W. Zhou, H. Fu, *ChemCatChem* **2013**, DOI: 10.1002/cctc.201200519; b) W. Zhou, F. Sun, K. Pan, G. Tian, B. Jiang, Z. Ren, C. Tian, H. Fu, *Adv. Funct. Mater.* **2011**, *21*, 1922–1930; c) S. A. El-Safty, M. A. Shenashen, *TrAC Trends Anal. Chem.* **2012**, *38*, 98–115.
- [3] a) S. A. El-Safty, M. A. Shenashen, A. A. Ismail, *Chem. Commun.* **2012**, *48*, 9652–9654; b) S. A. El-Safty, M. A. Shenashen, M. Ismael, M. Khairy, Md. R. Awual, *Analyst* **2012**, *137*, 5278–5290; c) S. A. El-Safty, Md. R. Awual, M. A. Shenashen, A. Shahat, *Sens. Actuators B* **2013**, *176*, 1015–1025; d) M. A. Shenashen, A. Shahat, S. A. El-Safty, *J. Hazard. Mater.* **2013**, *244–245*, 726–735; e) S. A. El-Safty, M. A. Shenashen, M. Ismael, M. Khairy, Md. R. Awual, *Microporous Mesoporous Mater.* **2013**, *166*, 195–205; f) S. A. El-Safty, A. Abdellatif, M. Ismael, A. Shahat, *Adv. Healthcare Mater.* **2013**, DOI: 10.1002/adhm.201200326; g) S. A. El-Safty, M. A. Shenashen, A. Shahat, *Small* **2013**, DOI: 10.1002/smll.201202407.
- [4] a) S. A. El-Safty, M. Mekawy, A. Yamaguchi, A. Shahat, K. Ogawa, N. Teramae, *Chem. Commun.* **2010**, *46*, 3917–3919; b) S. A. El-Safty, A. Shahat, M. Mekawy, H. Nguyen, W. Warkocki, M. Ohnuma, *Nanotechnology* **2010**, *21*, 375603; c) S. A. El-Safty, A. Shahat, W. Warkocki, M. Ohnuma, *Small* **2011**, *7*, 62–65; d) S. A. El-Safty, A. Shahat, Md. R. Awual, M. Mekawy, *J. Mater. Chem.* **2011**, *21*, 5593–5603; e) S. A. El-Safty, M. A. Shenashen, *Anal. Chim. Acta* **2011**, *694*, 151–161; f) S. A. El-Safty, A. Shahat, H. Nguyen, *Colloids Surf. A* **2011**, *377*, 44–53; g) S. A. El-Safty, N. D. Hoa, M. Shenashen, *Eur. J. Inorg. Chem.* **2012**, 5439–5450.
- [5] a) A. Corma, P. Atienzar, H. Garcia, J. Y. Chane-Ching, *Nat. Mater.* **2004**, *3*, 394–397; b) T. Waitz, T. Wagner, T. Sauerwald, C. D. Kohl, M. Tiemann, *Adv. Funct. Mater.* **2009**, *19*, 653–661.
- [6] W. Schmidt, *ChemCatChem* **2009**, *1*, 53–67.
- [7] a) S. A. El-Safty, M. Khairy, M. Ismael, H. Kawarada, *Appl. Catal. B* **2012**, *123–124*, 162–173; b) M. Khairy, S. A. El-Safty, *Curr. Catal.* **2013**, *2*, 17–26; c) S. Das, A. Goswami, N. Murali, T. Asefa, *ChemCatChem* **2013**, DOI: 10.1002/cctc.201200551; d) M. Khairy, S. A. El-Safty, M. Ismael, H. Kawarada, *Appl. Catal. B* **2012**, *127*, 1–10.
- [8] a) P. Yang, D. Zhao, D. I. Margolese, B. F. Chmelka, G. D. Stucky, *Chem. Mater.* **1999**, *11*, 2813–2826; b) S. A. El-Safty, *J. Porous Mater.* **2011**, *18*, 259–287; c) S. A. El-Safty, A. Shahat, K. Ogawa, T. Hanaoka, *Microporous Mesoporous Mater.* **2011**, *138*, 51–62; d) S. A. El-Safty, *J. Porous Mater.* **2008**, *15*, 369–387.
- [9] a) D. Wang, T. Xie, Q. Peng, Y. Li, *J. Am. Chem. Soc.* **2008**, *130*, 4016–4022; b) M. Khairy, S. A. El-Safty, M. Ismael, *Chem. Commun.* **2012**, *48*, 10832–10834.
- [10] S. K. Das, M. K. Bhunia, A. Bhaumik, *Dalton Trans.* **2010**, *39*, 4382–4390.
- [11] J. Y. Chane-Ching, F. Cobo, D. Aubert, H. G. Harvey, M. Airiau, A. Corma, *Chem. Eur. J.* **2005**, *11*, 979–987.
- [12] a) J. Ba, J. Polleux, M. Antonietti, M. Niederberger, *Adv. Mater.* **2005**, *17*, 2509–2512; b) C. Aprile, L. Teruel, M. Alvaro, H. Garcia, *J. Am. Chem. Soc.* **2009**, *131*, 1342–1343.
- [13] H. Chen, J. Gu, J. Shi, Z. Liu, J. Gao, M. Ruan, D. Yan, *Adv. Mater.* **2005**, *17*, 2010–2014.
- [14] S. K. Das, M. K. Bhunia, A. K. Sinha, A. Bhaumik, *J. Phys. Chem. C* **2009**, *113*, 8918–8923.
- [15] a) Y. S. Tao, H. Kanoh, L. Abrams, K. Kaneko, *Chem. Rev.* **2006**, *106*, 896–910; b) "Statistics. The EU biodiesel industry". *European Biodiesel Board*, **2008-03-28**. Retrieved 2008-04-03.
- [16] a) T. W. Kim, M. J. Kim, F. Kleitz, M. M. Nair, R. Guillet-Nicolas, K. E. Jeong, H. J. Chae, C. U. Kim, S. Y. Jeong, *ChemCatChem* **2012**, *4*, 687–697; b) G. Corro, U. Pal, N. Tellez, *Appl. Catal. B* **2013**, *129*, 39–47.
- [17] A. A. Kiss, A. C. Dimian, G. Rothenberg, *Energy Fuels* **2008**, *22*, 598–604.
- [18] a) J. Sheehan, V. Camobreco, J. Duffield, M. Graboski, H. Shapouri, *National Renewable Energy Laboratory: Golden, CO*, **1998**, 60; b) A. Demirbas, *Energy Explor. Exploit.* **2003**, *21*, 475–487.
- [19] a) W. Li, S. Choi, J. H. Drese, M. Hornbostel, G. Krishnan, P. M. Eisenberger, C. W. Jones, *ChemSusChem* **2010**, *3*, 899–903; b) U. S. Dept. of Energy. Clean Cities Alternative Fuel Price Report July **2009**. Retrieved 9-05-2009.
- [20] a) R. E. Teixeira, *Green Chem.* **2012**, *14*, 419–427; b) K. L. Kline, G. A. Olatosun, A. K. Wolfe, R. D. Perlack, V. H. Dale, M. McMahon, *Biofuel feedstock assessment for selected countries*, February, **2008**, Report No. ORNL/TM-2007/224, DOI: 10.2172/924080.

- [21] H. Fukuda, A. Kondo, H. Noda, *J. Biosci. Bioeng.* **2001**, *92*, 405–416.
- [22] N. Pal, M. Paul, A. Bhaumik, *J. Solid State Chem.* **2011**, *184*, 1805–1812.
- [23] M. Pramanik, M. Nandi, H. Uyama, A. Bhaumik, *Green Chem.* **2012**, *14*, 2273–2281.
- [24] E. Lotero, Y. Liu, D. E. Lopez, K. Suwannakarn, D. A. Bruce, J. G. Goodwin, *Ind. Eng. Chem. Res.* **2005**, *44*, 5353–5363.
- [25] a) J. M. Marchetti, A. F. Errazu, *Biomass Bioenergy* **2008**, *32*, 892–895; b) A. Macarioa, G. Giordanoa, B. Onida, D. Cocina, A. Tagarelli, A. M. Giuffrè, *Appl. Catal. A* **2010**, *378*, 160–168.
- [26] M. K. Bhunia, S. K. Das, P. Pachfule, R. Banerjee, A. Bhaumik, *Dalton Trans.* **2012**, *41*, 1304–1311.
- [27] J. C. Juan, J. Zhang, M. A. Yarmo, *Catal. Lett.* **2008**, *126*, 319–324.
- [28] A. A. Kiss, A. C. Dimian, G. Rothenberg, *Adv. Synth. Catal.* **2006**, *348*, 75–81.
- [29] A. C. Dimian, Z. W. Srokol, M. C. Mittelmeijer-Hazeleger, G. Rothenberg, *Top. Catal.* **2010**, *53*, 1197–1201.
- [30] a) R. Liu, X. Wang, X. Zhao, P. Feng, *Carbon* **2008**, *46*, 1664–1669; b) R. Luque, J. H. Clark, *ChemCatChem* **2011**, *3*, 594–597.
- [31] K. Saravanan, B. Tyagi, H. C. Bajaj, *Catal. Sci. Technol.* **2012**, *2*, 2512–2520.
- [32] a) A. Patel, V. Brahmkhatri, N. Singh, *Renewable Energy* **2013**, *51*, 227–233; b) W. Li, F. Ma, F. Su, L. Ma, S. Zhang, Y. Guo, *ChemCatChem* **2012**, *4*, 1798–1907.
- [33] Y. Sun, S. Ma, Y. Du, L. Yuan, S. Wang, J. Yang, F. Deng, F. S. Xiao, *J. Phys. Chem. B* **2005**, *109*, 2567–2572.
- [34] X.-R. Chen, Y.-H. Ju, C.-Y. Mou, *J. Phys. Chem. C* **2007**, *111*, 18731–18737.
- [35] R. Sánchez-Vázquez, C. Pirez, J. Iglesias, K. Wilson, A. F. Lee, J. A. Melero, *ChemCatChem* **2013**, DOI: 10.1002/cctc.201200527.
- [36] a) S. Blagov, S. Parada, O. Bailer, P. Moritz, D. Lam, R. Weinand, H. Hasse, *Chem. Eng. Sci.* **2006**, *61*, 753–765; b) D. Fang, J. Yang, C. Jiao, *ACS Catal.* **2011**, *1*, 42–47.
- [37] K. N. Rao, A. Sridhar, A. F. Lee, S. J. Tavener, N. A. Young, K. Wilson, *Green Chem.* **2006**, *8*, 790–797.
- [38] a) M. I. López, D. Esquivel, C. Jiménez-Sanchidrián, F. J. Romero-Salguero, *ChemCatChem* **2013**, DOI: 10.1002/cctc.201200509; b) T. Yalçinyuva, H. Deligöz, I. Boz, M. A. Gürkaynak, *Int. J. Chem. Kinet.* **2008**, *40*, 136–144.
- [39] Y. F. Feng, X. Y. Yang, D. Yang, Y. C. Du, Y. L. Zhang, F. S. Xiao, *J. Phys. Chem. B* **2006**, *110*, 14142–14147.
- [40] S. K. Das, M. K. Bhunia, A. K. Sinha, A. Bhaumik, *ACS Catal.* **2011**, *1*, 493–501.
- [41] S. K. Das, M. K. Bhunia, A. Bhaumik, *Open Catal. J.* **2012**, *5*, 56–65.
- [42] B. M. Reddy, P. M. Sreekanth, P. Lakshmanan, *J. Mol. Catal. A-Chem.* **2005**, *237*, 93–100.
- [43] J. R. Sohn, T. D. Kwon, S. B. Kim, *Bull. Korean Chem. Soc.* **2001**, *22*, 1309–1315.
- [44] Y. S. Hsu, Y. L. Wang, A. N. Ko, *J. Chin. Chem. Soc.* **2009**, *56*, 314–322.
- [45] S. A. El-Safty, M. A. Shenashen, M. Ismael, M. Khairy, *Adv. Funct. Mater.* **2012**, *22*, 3013–3021.
- [46] W. Yue, A. H. Hill, A. Harrison, W. Zhou, *Chem. Commun.* **2007**, 2518–2520.
- [47] a) L. Kundakovic, M. Flytzani-Stephanopoulos, *Appl. Catal. A* **1999**, *183*, 35–51; b) A. Bensalem, J. C. Muller, F. Bozon-Verduraz, *J. Chem. Soc. Faraday Trans.* **1992**, *88*, 153–154.
- [48] S. K. Das, M. K. Bhunia, M. M. Seikh, S. Dutta, A. Bhaumik, *Dalton Trans.* **2011**, *40*, 2932–2939.
- [49] J. R. Sohn, S. H. Lee, J. S. Lim, *Catal. Today* **2006**, *116*, 143–150.
- [50] B. A. Morrow, R. A. McFarlane, M. Lion, J. C. Lavalley, *J. Catal.* **1987**, *107*, 232–239.
- [51] T. Yamaguchi, T. Jin, K. Tanabe, *J. Phys. Chem.* **1986**, *90*, 3148–3152.
- [52] a) B. M. Reddy, M. K. Patil, *Chem. Rev.* **2009**, *109*, 2185–2206; b) M. K. Lam, K. T. Lee, A. R. Mohamed, *Biotechnol. Adv.* **2010**, *28*, 500–518.
- [53] A. Sivasamy, K. Y. Cheah, P. Fornasiero, F. Kemausuor, S. Zinoviev, S. Mierthus, *ChemSusChem* **2009**, *2*, 278–300.
- [54] A. S. Deshpande, N. Pinna, P. Beato, M. Antonietti, M. Niederberger, *Chem. Mater.* **2004**, *16*, 2599–2604.

Received: March 16, 2013

Published online on ■ ■ ■ ■, 0000